SOLUTION OF RADIATION PROBLEMS WITH EXACT GEOMETRY

by C.-H. Lee[1] and J. N. Newman[2]
[1] WAMIT, Inc., Chestnut Hill, MA USA (chlee@wamit.com)
[2] MIT, Cambridge, MA USA (jnn@mit.edu)

(16th Workshop on Water Waves and Floating Bodies – Hiroshima, Japan – 22-25 April 2001)

The panel method is used frequently to solve three-dimensional radiation and diffraction problems in the frequency domain. In the usual numerical procedure the submerged surface of the body is represented by small elements. Both the solution for the velocity potential or source strength, and also the body geometry, are approximated on each element.

In most practical cases the number of elements needed to achieve the desired accuracy is large, on the order of 1000. Significant effort may be required to develop a suitable set of elements for input to the program. Generally this requires the use of special pre-processing software. Several input files with systematically smaller elements may be required to establish convergence. Despite these problems, the low-order panel method is widely used for radiation/diffraction analyses, even for simple bodies such as spheres and cylinders.

It is not strictly necessary to approximate the body geometry, if it can be represented explicitly in the program. This avoids the effort of developing appropriate input files with small elements, and provides a more accurate description of the geometry. The explicit representation is most useful in conjunction with a higher-order representation of the solution. Some modifications are required in the numerical implementation and coding, particularly with respect to the evaluation of the influence functions.

In some cases one explicit algorithm is sufficient to describe the entire body surface. A much wider class of bodies can be represented by subdividing the submerged surface into patches, with separate algorithms corresponding to each patch. The truncated circular cylinder is an example, where two separate patches are required to represent the cylindrical side and circular flat bottom. The fundamental property of each patch is that its surface is smooth, continuous, and differentiable. The most general definition of the class of bodies we include here is that the submerged surface can be subdivided into a set of patches, where a pair of parametric coordinates (u, v) is used to define the position on each patch, the boundaries of the patch map to a square in the parametric space, and an explicit transformation $\mathbf{x}(u, v)$ exists between the Cartesian space (x, y, z) and the parametric space.

This procedure has been used to extend the capabilities of the radiation/diffraction code WAMIT. Except for the use of explicit geometry we follow the approach developed by Maniar (1995), and described by Lee *et al* (1996). In that work B-splines are used to represent both the geometry and the velocity potential on each patch. Here we use B-splines only to represent the velocity potential. The accuracy of the solution can be systematically refined by controlling the degree of the B-splines, and/or subdividing each patch into 'panels' with B-spline knots at the panel boundaries. Three examples follow, with brief descriptions of the body representation and hydrodynamic results.

Truncated vertical cylinder with an oblate spheroidal bottom

The family of bodies shown in Figure 1 is generated by a simple subroutine. Quadratic B-splines are used to represent the solution. On each patch, 2×2 or 4×4 panels are used. In the case $R = 0$, corresponding to a submerged oblate spheroid, one patch is used with 16 or 36 unknowns. In the cases $R > 0$ two patches are used and the total number of unknowns (B-spline coefficients) is 32 or 72, respectively.

Figure 2 shows the heave added-mass and damping coefficients. For the three intermediate cases ($R = 0.25$, 0.5, 0.75) the damping coefficient (and also the heave exciting force) vanish at ($k = 0.045$, 0.22, 0.74), respectively.

The McIver toroid

The McIver toroid shown in Figure 3 was analyzed by Newman (1999), using the low-order panel method. The results of that work confirmed the existence of a singular solution at the first zero of the Bessel function $J_0(k)$ ($k = 2.4048$). However the convergence of the low-order analysis is relatively slow near the singular wavenumber, and up to 8192 panels were used (2048 unknowns). For the present higher-order analysis an explicit representation of the geometry has been developed. The procedure described by Newman (1999) is used to compute the loci of points on a cross-section. These points are expressed in terms of the toroidal coordinates R and θ about the axis of the ring source and the radius $R(\theta)$ is approximated by an economized polynomial of degree 10. The maximum error in this approximation is a radial difference on the order of 0.00001. Only one patch is required to represent one quadrant of the toroid, as shown in Figure 3. Quadratic B-splines are used to represent the velocity potential.

Figure 4 shows the heave added mass in the vicinity of the singular wavenumber, and the convergence of the singular wavenumber with increasing numbers of panels using both the low- and higher-order methods. (The singular wavenumber is defined here as the value of k where the added-mass coefficient changes sign from positive to negative values.) It is apparent that the higher-order solution is more accurate, and requires a much smaller number of unknowns.

Rectangular barge with moonpool

A rectangular barge with two planes of symmetry and a rectangular moonpool at its center is represented by six flat rectangular patches (end, side, moonpool end, moonpool side, bottom forward of the moonpool, and bottom outboard of the moonpool). The principal dimensions are length=16m, beam=4m, moonpool length 8m, and moonpool width 2m. The draft is varied between 0.125m and 2.0m to illustrate its effect on the moonpool resonant frequencies. The table below shows the peak amplitude and wavenumber for the first five Fourier coefficients of the free-surface elevation in the moonpool. In the 'radiation' data the barge oscillates in the surge/heave modes in calm water, and the Fourier coefficients are evaluated directly from the resulting free-surface elevation on the centerline of the moonpool. In the 'diffraction' data the barge is fixed in incident head waves. Most of the resonant amplitudes are greater in the radiation problem, due to the stronger forcing by the body motions.

The last line in the table shows the asymptotic limits of the resonant wavenumbers for infinite draft. In this limit the resonant modes $n > 0$ correspond to standing waves with n nodes, in a basin with the same horizontal dimensions as the moonpool. As the draft is reduced the resonant wavenumber increases, corresponding to a reduction in the resonant wave period. This was first noted and explained by Molin (1999). For the 'pumping mode' ($n = 0$) the resonant wavenumber $k \simeq 1/T$ for large draft T.

	draft(m)	k_0	$\|c_0\|$	k_1	$\|c_1\|$	k_2	$\|c_2\|$	k_3	$\|c_3\|$	k_4	$\|c_4\|$
radiation:	0.125	0.82	3.0	1.00	0.4	1.27	14	1.60	5.1	1.93	89
	0.25	0.76	3.0	0.92	1.1	1.18	15	1.49	16	1.82	127
	0.5	0.64	3.2	0.78	3.4	1.03	21	1.34	84	1.68	310
	1.0	0.48	3.9	0.62	16	0.89	56	1.22	1115	1.59	465
	2.0	0.32	5.0	0.48	127	0.81	500	1.18	35000	1.57	3300
diffraction:	0.125					1.28	0.6	1.61	1.0	1.95	1.0
	0.25			0.92	1.1	1.18	1.1	1.49	2.3	1.82	3.8
	0.5			0.78	1.3	1.03	3.1	1.34	7.2	1.68	16
	1.0	0.46	1.0	0.62	4.3	0.89	12	1.22	32	1.59	91
	2.0	0.31	3.5	0.48	17	0.81	72	1.18	572	1.57	225
	∞	0		0.39		0.79		1.17		1.57	

Table 1: Resonant wavenumbers k_n and amplitudes $|c_n|$ of Fourier modes in the moonpool of a rectangular barge. The last line shows the infinite-draft limits.

REFERENCES

Lee, C.-H., Maniar, H., Newman, J., & Zhu, X. 1996. 'Computations of wave loads using a B-spline panel method,' *Proc. 21st Symp. on Naval Hydrodynamics,* Trondheim, pp. 75-92.

Maniar, H. 1995. *A three dimensional higher order panel method based on B-splines,* Ph.D. thesis, MIT.

Molin, B., 2000. 'On the sloshing modes in moonpools, or the dispersion equation for progressive waves in a channel through the ice sheet,' *Proc. 15th Intl. Workshop on Water Waves and Floating Bodies,* Caesaria, Israel, pp. 122-125.

Newman, J. N. 1999. 'Radiation and diffraction analysis of the McIver toroid,' *J. of Engineering Maths.* Vol. 35, pp. 135-147.

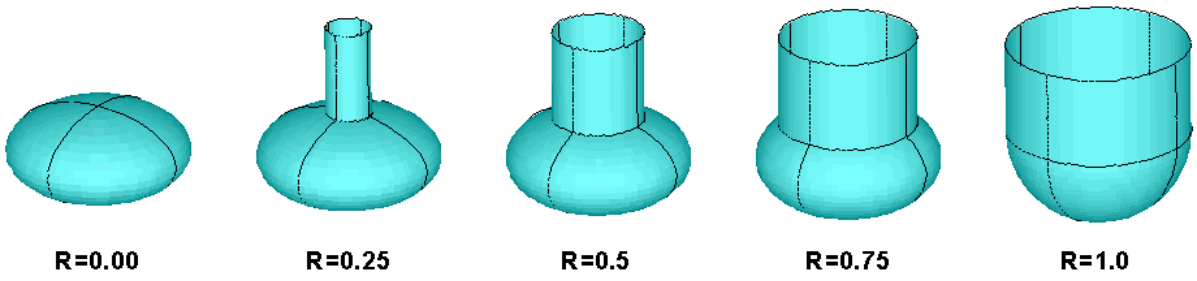

Figure 1: Perspective views of the truncated vertical cylinder of radius $R \le 1$, extending from the free surface ($z = 0$) to $z = -1$, with an oblate spheroidal bottom which has a radius equal to 1.0, and extends from $z = -1$ to $z = -2$. The boundaries of the patches and their images are shown by dark lines.

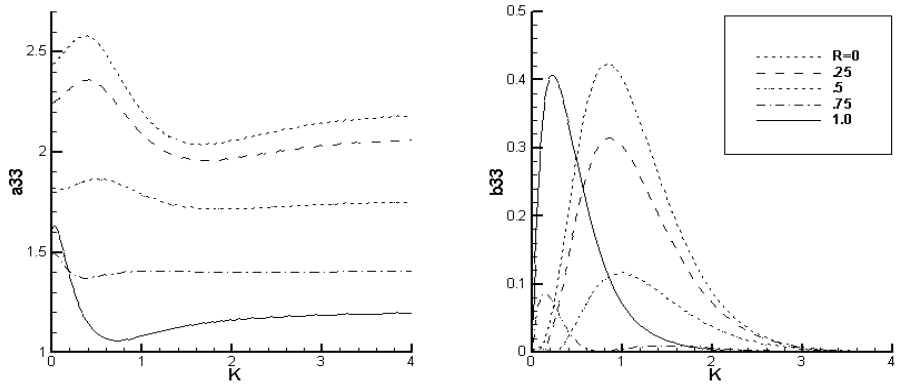

Figure 2: Heave added-mass and damping coefficients for the family of bodies shown in Figure 1.

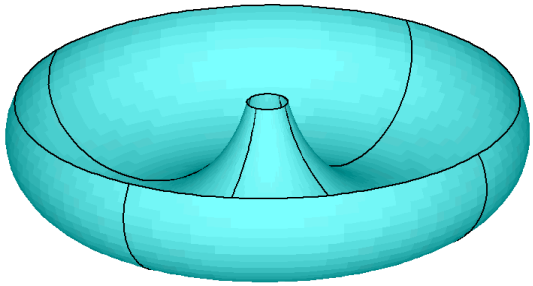

Figure 3: Perspective view of the McIver toroid generated by a ring source of unit radius, with the inner waterline at $r = 0.2$ and the outer waterline at $r = 2.4687$.

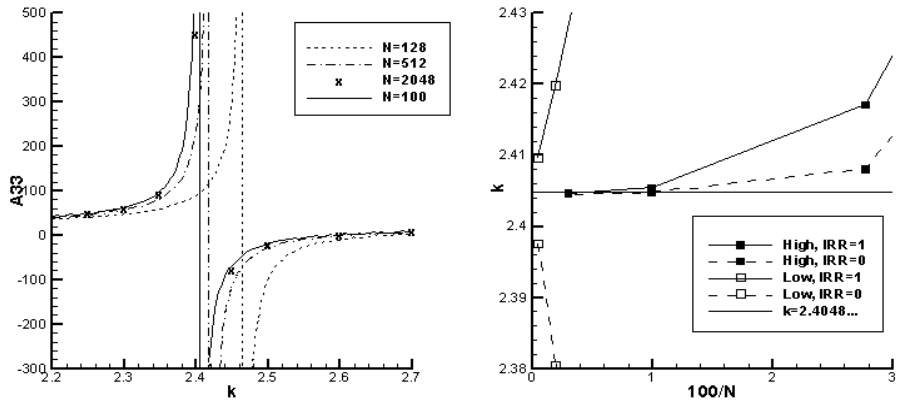

Figure 4: Results for the McIver toroid. The left figure shows the heave added-mass coefficient, including results from the low-order analysis with N=128, 512, 2048 panels on one quadrant of the body surface, and the higher-order results with explicit geometry definition (N=100 unknowns). The latter results are converged within graphical accuracy. The right figure shows the convergence of the low- and higher-order results to the singular wavenumber $J_0(k) = 0$. IRR=1 denotes that the irregular-frequency effects are removed.